



Dynamics of the binary asteroid (379) Huenna

Frédéric Vachier, Benoit Carry, Jérôme Berthier

► To cite this version:

Frédéric Vachier, Benoit Carry, Jérôme Berthier. Dynamics of the binary asteroid (379) Huenna. Icarus, 2022, 382, 10.1016/j.icarus.2022.115013 . insu-03656890

HAL Id: insu-03656890

<https://insu.hal.science/insu-03656890v1>

Submitted on 22 Jul 2024

HAL is a multi-disciplinary open access archive for the deposit and dissemination of scientific research documents, whether they are published or not. The documents may come from teaching and research institutions in France or abroad, or from public or private research centers.

L'archive ouverte pluridisciplinaire **HAL**, est destinée au dépôt et à la diffusion de documents scientifiques de niveau recherche, publiés ou non, émanant des établissements d'enseignement et de recherche français ou étrangers, des laboratoires publics ou privés.



Distributed under a Creative Commons Attribution - NonCommercial 4.0 International License

Dynamics of the binary asteroid (379) Huenna

*Corresponding author

 frederic.vachier@obspm.fr (F. Vachier)

ORCID(s): 0000-0002-4289-4466 (F. Vachier); 0000-0001-5242-3089 (B. Carry); 0000-0003-1846-6485 (J. Berthier)

Frédéric Vachier^{a,*}, Benoit Carry^b and Jérôme Berthier^a

^aIMCCE, Observatoire de Paris, PSL Research University, CNRS, Sorbonne Universités, UPMC Univ Paris 06, Univ. Lille, France

^bUniversité Côte d'Azur, Observatoire de la Côte d'Azur, CNRS, Laboratoire Lagrange, France

ARTICLE INFO

Keywords:
dynamics
external perturbers
bulk density

ABSTRACT

We aim at studying the dynamical system of the asteroid (379) Huenna and its satellite, for which a discrepancy between its predicted and observed position was reported by DeMeo et al. (2011, Icarus, 212). We compile all the available images of the system acquired with large ground-based telescopes equipped with adaptive-optics fed camera. Based on these 40 observations covering 11 years, we determine the orbit of the satellite which is strongly affected by the gravitational influence of the Sun, as opposed to most satellites of large main-belt asteroids. Combining the mass of Huenna with a compilation of diameter estimates from the literature, we revise the estimate of its bulk density to $1491 \pm 249 \text{ kg}\cdot\text{m}^{-3}$, consistent with its spectral classification as a P-type asteroid.

1. Introduction

Owing to their small size, asteroids had little, if any, geophysical evolution over the history of the Solar system after their initial accretion phase some 4.6 Gyr ago. Their orbital environment, dominated by collisions, however led to an important evolution of their physical properties such as spin, shape, and internal structure via shock-induced fractures. Asteroids are nevertheless the most pristine remnants of the early stages of the inner Solar system, and as such, they are used to constrain the models of formation and evolution of planetesimals from which terrestrial planets formed (Morbidelli et al., 2015; Clement et al., 2020)

Understanding their compositions, and how these distribute is key in that respect (DeMeo and Carry, 2014). The composition of asteroids is generally derived from photometry and spectroscopy compared with laboratory samples (Reddy et al., 2015). These are, however, sensitive to a thin surface layer only, which composition may or may be not related to the bulk composition of the asteroid. An obvious example is the differentiated asteroid (4) Vesta (McCord et al., 1970), but partially differentiated bodies could be common (Elkins-Tanton et al., 2011; Bryson et al., 2019). Asteroid bulk density is the sole remote-sensing quantity that can tell us about asteroid interiors, and provide hints on bulk composition (Scheeres et al., 2015).

The first and most difficult quantity to measure to derive an asteroid density is its mass. The only exception is the modeling of lightcurves of mutual events (eclipses and occultations) which provides the density without measuring the asteroid mass (nor volume, see Pravec et al., 2006; Scheirich and Pravec, 2009; Carry et al., 2015). In all cases, the most precise mass estimates (few percent accuracy) have been derived studying binary asteroids, or during spacecraft encounters (Pätzold et al., 2011; Pajuelo et al., 2018). Other determinations, relying on the modeling of the long-distance

gravitational influence of the target asteroids on other small asteroids, have provided many more determination but with low precision to date (Zielenbach, 2011). There are currently about 300 small bodies with a mass determination (Carry, 2012).

We focus here on the asteroid (379) Huenna, around which a satellite was discovered in 2003 by Margot (2003). A dynamical solution for the orbit of the satellite was published by Marchis et al. (2008), providing the mass of Huenna. However, the observation in 2009 of Huenna's satellite for spectroscopic purposes revealed a clear offset (0.5'', about 680 km) between the predicted and observed positions (DeMeo et al., 2011), requiring an updated dynamical solution. A dynamical solution has indeed been recently published by Emelyanov and Drozdov (2020) based on the aforementioned observations. Aware of additional observations present in archives, we collected images of Huenna's system as acquired by large ground-based telescopes in Section 2. We then describe the dynamical solution in Section 3, and discuss its implications in Section 4.

2. Observations and data reduction

We collect all the high angular-resolution images of Huenna taken with ground-based telescopes equipped with adaptive-optics (AO) cameras: ESO VLT and W. M. Keck. The data span 27 different epochs, with multiple images each, over 11 years from August 2003 to December 2014. This data set includes the discovery observations of Margot (2003), those used by Marchis et al. (2008), the discrepant observation reported by DeMeo et al. (2011), and public data from the archives of the Keck (Keck engineering time and programs C257N2L, C192N2, PI M. Brown) and VLT telescopes (program 089.C-0944, PI F. Marchis).

The images from the VLT were acquired with NACO (NAOS-CONICA, Lenzen et al., 2003; Rousset et al., 2003), and those at Keck with NIRCam (Near-Infrared

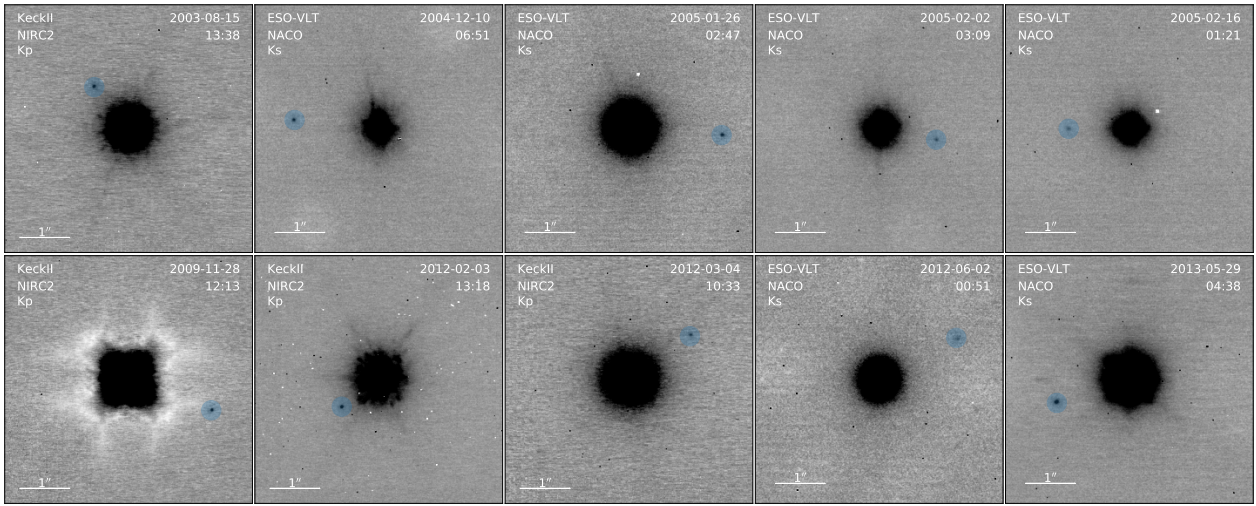


Figure 1: Examples of AO images. The small blue circles indicate the position of the satellite. North is up and East is left.

Camera 2, van Dam et al., 2004; Wizinowich et al., 2000). We reduce the AO imaging data with a standard data processing protocol (sky subtraction, bad-pixel identification and correction, and flat-field correction), using in-house routines (see Carry et al., 2008). The reduced images were processed to subtract the bright halo surrounding Huenna to enhance the detectability of its satellite (see Pajuelo et al., 2018, for details). The measured positions of the satellite are listed in Table 1, and we present a few examples in Figure 1.

3. Orbit of the satellite

We use all 40 positions of the satellite with respect to Huenna on the plane of the sky to characterize its orbital properties. We use the Genoid algorithm to find the set of dynamical parameters (mass, semi-major axis, eccentricity, inclination, longitude of the node, argument of pericenter, and time of passage to pericenter) that best fit the observations (see Vachier et al., 2012; Berthier et al., 2014; Carry et al., 2019, 2021, for a detailed description of the algorithm and application to different systems).

Genoid explores the parameter space by successives generations of suites of test solutions (called individuals). Each test solution consists in the set of dynamical parameters, and is compared with observations through numerical integration of the system, with the following metric:

$$\chi^2 = \sum_{i=1}^N \left[\left(\frac{X_{o,i} - X_{c,i}}{\sigma_{x,i}} \right)^2 + \left(\frac{Y_{o,i} - Y_{c,i}}{\sigma_{y,i}} \right)^2 \right] \quad (1)$$

where N is the number of observations, and X_i and Y_i are the relative positions between the satellite and Huenna along the right ascension and declination, respectively. The indices o and c stand for observed and

computed positions, and σ are the measurement uncertainties.

At each generation, the individuals with the lowest χ^2 are used to generate the individuals of the following generation, by randomly mixing their parameters (like sexual reproduction mixes genes). At each generation, the best solution is also used as initial condition to search for the local minimum by gradient descent. The algorithm stops after a given number of generations, or when the χ^2 achieved by several generations does not evolve anymore.

The combination of both a large grid search and a gradient descent ensures finding the best global dynamical solution. The numerical integration is handled by eproc, the library of ephemerides computation behind all the Virtual Observatory Web services of the IMCCE (e.g., SkyBoT, Miriade, Berthier et al., 2006, 2008, 2016). As such, it is a one body integrator perturbed by N-bodies and has been extensively tested.

The numerical model used here consists in Huenna and its satellite, and the Sun. The case of Huenna differs from other large asteroids with satellite for which the perturbation by the Sun (or any planet) is negligible. Recent studies revealed purely Keplerian motions around (22) Kalliope, (31) Euphrosyne, (41) Daphne, (87) Sylvia, (107) Camilla, (130) Elektra, and (317) Roxane (Drummond et al., 2021; Yang et al., 2020; Carry et al., 2019, 2021; Berthier et al., 2014; Beauvalet and Marchis, 2014; Pajuelo et al., 2018; Yang et al., 2016). Considering the distribution of the separation between asteroids and their satellites (Fig. 2, data from Johnston 2019), only the outer satellite of (3749) Balam and the satellite of (379) Huenna are distant. The satellites of other bodies are located much deeper into their respective Hill spheres.

The influence of the Sun on the position of the satellite of Huenna is well above the typical precision of

Table 1

Astrometry of the satellite of Huenna. Date, mid-observing time (UTC), telescope, camera, filter, astrometry (X is aligned with Right Ascension, and Y with Declination, and o and c indices stand for observed and computed positions), uncertainty (σ), and photometry (magnitude difference ΔM with uncertainty δM) are reported.

Date	UTC	Tel.	Cam.	Filter	X_o (mas)	Y_o (mas)	X_{o-c} (mas)	Y_{o-c} (mas)	σ (mas)	ΔM (mag)	δM (mag)
2003-08-14	13:04:25.9	Keck-II	NIRC2	H	501	737	1	3	10.00	8.14	0.56
2003-08-14	14:07:52.8	Keck-II	NIRC2	H	506	737	-2	0	10.00	7.76	0.27
2003-08-15	13:34:46.6	Keck-II	NIRC2	Kp	693	838	1	0	10.00	6.98	0.07
2003-08-15	13:38:59.6	Keck-II	NIRC2	Kp	696	841	3	3	10.00	7.13	0.06
2003-08-17	14:53:55.0	Keck-II	NIRC2	Kp	1070	1028	1	-7	10.00	7.10	0.11
2003-08-18	14:19:56.0	Keck-II	NIRC2	Kp	1243	1116	2	-6	10.00	6.94	0.03
2004-12-08	07:08:31.3	ESO VLT	NACO	Ks	1783	130	4	4	13.30	7.43	0.80
2004-12-09	06:29:18.8	ESO VLT	NACO	Ks	1759	147	14	-2	13.30	6.55	0.41
2004-12-09	06:41:52.7	ESO VLT	NACO	Ks	1743	146	-1	-3	13.30	6.88	0.03
2004-12-10	06:45:20.8	ESO VLT	NACO	Ks	1702	176	1	1	13.30	6.37	0.56
2004-12-10	06:51:28.8	ESO VLT	NACO	Ks	1697	174	-2	0	13.30	6.67	0.03
2004-12-14	05:28:42.9	ESO VLT	NACO	Ks	1447	264	-1	2	13.30	6.65	0.07
2004-12-14	07:08:56.9	ESO VLT	NACO	Ks	1448	266	5	2	13.30	6.73	0.05
2004-12-15	05:20:24.8	ESO VLT	NACO	Ks	1370	285	1	3	13.30	6.87	0.13
2004-12-28	05:36:53.1	ESO VLT	NACO	Ks	-21	396	3	3	13.30	7.06	0.32
2004-12-28	07:41:12.8	ESO VLT	NACO	Ks	-41	397	-6	4	13.30	6.96	0.43
2004-12-29	05:13:34.3	ESO VLT	NACO	Ks	-141	391	0	0	13.30	6.28	0.00
2005-01-18	03:58:33.8	ESO VLT	NACO	Ks	-1924	65	4	7	13.30	7.03	0.07
2005-01-18	06:17:33.1	ESO VLT	NACO	Ks	-1931	56	0	1	13.30	6.72	0.13
2005-01-21	02:25:25.0	ESO VLT	NACO	Ks	-1991	-15	-4	0	13.30	6.79	0.51
2005-01-25	04:51:31.4	ESO VLT	NACO	Ks	-1916	-110	-2	0	13.30	7.44	0.00
2005-01-26	02:47:39.2	ESO VLT	NACO	Ks	-1868	-127	0	2	13.30	6.88	0.03
2005-01-26	05:10:41.1	ESO VLT	NACO	Ks	-1860	-127	3	3	13.30	7.42	0.28
2005-01-27	03:10:50.5	ESO VLT	NACO	Ks	-1799	-146	7	2	13.30	7.13	0.20
2005-01-28	03:04:35.7	ESO VLT	NACO	Ks	-1734	-166	-1	1	13.30	6.74	0.34
2005-01-28	03:13:54.0	ESO VLT	NACO	H	-1735	-159	-3	7	13.30	7.37	0.15
2005-02-02	03:09:16.2	ESO VLT	NACO	Ks	-1147	-222	1	0	13.30	7.09	0.03
2005-02-02	05:09:29.4	ESO VLT	NACO	Ks	-1134	-225	2	-3	13.30	7.00	0.08
2005-02-04	02:41:04.7	ESO VLT	NACO	Ks	-823	-223	5	0	13.30	7.02	0.20
2005-02-04	04:05:56.8	ESO VLT	NACO	Ks	-819	-224	0	0	13.30	6.84	0.12
2005-02-16	01:21:08.5	ESO VLT	NACO	Ks	1221	-4	-3	-2	13.30	6.72	0.27
2009-11-28	12:13:35.1	Keck-II	NIRC2	Kp	-1672	-616	-4	4	10.00	7.16	0.08
2009-11-28	12:51:36.2	Keck-II	NIRC2	Kp	-1673	-615	-7	3	10.00	6.97	0.03
2012-02-03	13:18:43.9	Keck-II	NIRC2	Kp	740	-551	-7	-3	10.00	6.94	0.43
2012-02-03	13:33:28.7	Keck-II	NIRC2	Kp	739	-552	-8	-5	10.00	6.98	0.09
2012-03-04	10:33:13.8	Keck-II	NIRC2	Kp	-1225	894	4	19	10.00	7.37	0.28
2012-03-29	07:16:52.3	Keck-II	NIRC2	Kp	-1881	656	0	5	10.00	6.93	0.03
2012-06-02	00:51:58.5	ESO VLT	NACO	Ks	-1568	825	-12	-16	13.30	7.01	0.31
2014-11-10	07:16:10.7	Keck-II	NIRC2	Ks	3079	1085	-5	-16	10.00	1.65	0.06
2014-12-07	05:38:57.2	Keck-II	NIRC2	Ks	-554	-585	-2	-2	10.00	6.65	0.01
					Average	0	0			6.86	0.18
					Standard deviation	4	6			0.90	0.17

measurements, around $0.01''$ (Table 1). By comparing the best-fit solution (see below) including the Sun and a simple Keplerian orbit, we find a root mean-square residual of $0.477''$ over the period of 11 years covered by the observations, the two orbit diverging with time (Figure 3). The second-largest external perturber is Jupiter, but only contributes at the level of $0.0001''$ and we neglect it in our dynamical model.

We present in Table 2 the best-fitting orbital solu-

tion, providing a root mean-square deviation of only **5.4 milli-arcsconds (mas)**. This orbit significantly differs from the original dynamical solution of Marchis et al. (2008). While the orientation of the orbit (node, inclination, pericenter) is similar within a few degrees, the orbital period strongly disagree: **80.2 ± 0.01 d** here, compared to the previous value of **87.6 ± 0.26 d**; i.e., an increase of **9%**, at more than **28 σ** .

Four arguments argue in favor of the revised solu-

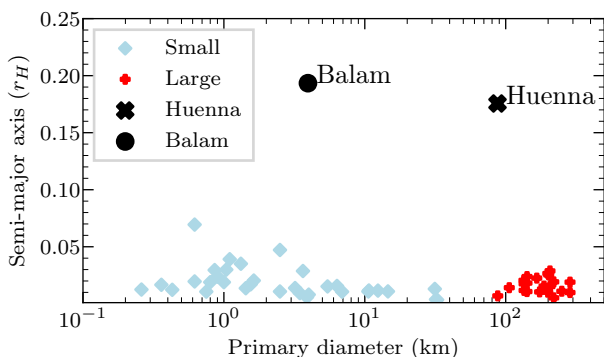


Figure 2: Semi-major axes of binary asteroids (expressed in radius of the Hill's sphere: r_H) as function of the diameter of the main component. The population is split into small (blue) and large (red) systems, using a diameter of 30 km to separate them.

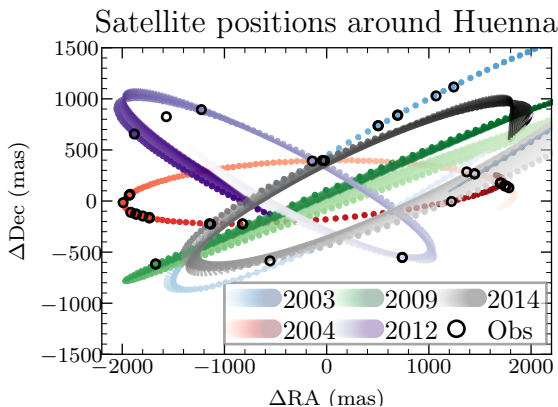


Figure 3: Comparison of the predicted position from a Keplerian orbit (fit over all 31 positions between 2003 and 2005 with a RMS of 3.6 mas only) and the orbit including the influence of the Sun. The black dots are the observations. The predictions of the two orbits are connected by lines, color-coded by epoch. The later the epoch the larger the difference.

among estimates, resulting in 10% uncertainty. This is expected for estimates based on the analysis of mid-infrared fluxes using a spherical assumption on the shape of asteroids (Mainzer et al., 2011; Carry, 2012; Usui et al., 2014; Herald et al., 2020). The updated mass and diameter estimates imply a bulk density of $1491 \pm 249 \text{ kg}\cdot\text{m}^{-3}$. This density is typical for a P-type (see, e.g., Carry, 2012; Berthier et al., 2014; Pajuelo et al., 2018; Carry et al., 2021; Vernazza et al., 2021). The diameter estimates are, however, only based on disk-integrated measurements, and the density estimate should hence be interpreted with caution.

Assuming that Huenna and its satellite have the same albedo (a reasonable assumption considering their similar spectra, see DeMeo et al., 2011), their apparent magnitude difference of 6.9 ± 0.9 (Table 1) implies a diameter of 3.72 ± 0.60 km only for the satellite. It is thus one of the smallest satellites of large ($50+ \text{ km}$) asteroids known to date, with Daphne, Elektra, and Minerva (Marchis et al., 2013; Yang et al., 2016; Carry et al., 2019).

Small satellites of large asteroids are thought to form in giant collisions (Durda et al., 2004; Margot et al., 2015), and share common properties. Their orbits tend to be equatorial, circular, in the direct sense, and deep within their Hill spheres (0.017 ± 0.002). The peculiar properties of the satellite of Huenna, especially its eccentricity and large semi-major axis, questions its origin, or evolution. While the likelihood of an origin by capture is low (Weidenschilling et al., 1989), what excited its orbit and increased its eccentricity and semi-major axis if formed like other satellites of large asteroids? The spin axis of Huenna is not known, and lightcurve observations of Huenna to determine it will help understanding the geometry of the system: whether the mutual orbit is equatorial or tilted.

5. Conclusion

We searched for adaptive-optics images of the asteroid (379) Huenna in the archives of large ground-based telescopes. We measured 40 positions of the satellite with respect to Huenna taken over 11 years. From these positions, we determined the dynamics of the satellite, solving the miss-match between previously published orbit and an observation in 2009. We derived a new estimate of the mass of Huenna. Combined with its average diameter computed from estimates reported in the literature, we determined a density of $1491 \pm 249 \text{ kg}\cdot\text{m}^{-3}$, typical of the P-types asteroids like Huenna. The satellite is on an eccentricity orbit, far from Huenna, which contrasts with the properties of most known satellites around large main-belt asteroids. A physical characterization of Huenna, and in particular of its spin axis, is required to study further the origin of this system.

tion: the agreement within 3σ between our dynamical solution and the recent study by Emelyanov and Drozdov (2020), the small residuals obtained here, the poor prediction of previous solution for the 2009 observation reported by DeMeo et al. (2011), and the time coverage of only 70 d used by Marchis et al. (2008), i.e., shorter than an orbital period.

4. Discussion

The revised dynamical solution implies a significantly larger mass (36%) compared to the previous determination (Marchis et al., 2008). In what follows, we assume that all the mass of the system is in Huenna, owing to the small size of its satellite (see below). We compile all the diameter estimates available in the literature in Table 3, and estimate an average diameter of 87.5 ± 8.2 km. There is a significant spread

Table 2

Orbital elements and state vector (centered on Huenna) of the satellite of Huenna, expressed in EQJ2000: orbital period P , semi-major axis a , eccentricity e , inclination i , longitude of the ascending node Ω , argument of pericenter ω , time of pericenter t_p . The number of observations and RMS between predicted and observed positions are also provided. Finally, we report the system total mass M , the ecliptic J2000 coordinates of the orbital pole (λ_p, β_p), and the equatorial J2000 coordinates of the orbital pole (α_p, δ_p). Uncertainties are given at 3σ .

Observing data set		
Number of observations	40	
Time span (days)	4133	
RMS (mas)	5.4	
Orbital elements EQJ2000		
P (day)	80.216	± 0.015
a (km)	3487.9	± 41.4
e	0.283	± 0.010
i ($^{\circ}$)	151.19	± 0.68
Ω ($^{\circ}$)	204.53	± 1.19
ω ($^{\circ}$)	278.9	± 1.5
t_p (JD)	2452930.961	± 0.31
State vector EQJ2000		
x (m)	-3 228 767.0	
y (m)	-621 087.4	
z (m)	426 401.0	
v_x (m/s)	-1.2471	
v_y (m/s)	2.6316	
v_z (m/s)	1.6019	
Derived parameters		
M ($\times 10^{17}$ kg)	5.23	± 0.19
α_p, δ_p ($^{\circ}$)	114.5, -61.2	$\pm 1.2, 0.7$
λ_p, β_p ($^{\circ}$)	161.8, -77.8	$\pm 3.4, 0.5$

Acknowledgments

Some of the work presented here is based on observations collected at the European Organisation for Astronomical Research in the Southern Hemisphere under ESO program 074.C-0052 and 089.C-0944 (PI Marchis).

Some of the data presented herein were obtained at the W.M. Keck Observatory, which is operated as a scientific partnership among the California Institute of Technology, the University of California and the National Aeronautics and Space Administration. The Observatory was made possible by the generous financial support of the W.M. Keck Foundation. This research has made use of the Keck Observatory Archive (KOA), which is operated by the W. M. Keck Observatory and the NASA Exoplanet Science Institute (NExScI), under contract with the National Aeronautics and Space Administration. The authors wish to recognize and acknowledge the very significant cultural role and reverence that the summit of Mauna Kea has always had within the indigenous Hawaiian community.

B. Carry was supported by CNRS/INSU/PNP. The

Table 3

Diameter estimates of Huenna compiled from the literature.

Diameter (km)	Method	Reference
92.33 \pm 1.70	STM	Tedesco et al. (2001)
103.01 \pm 4.31	NEATM	Ryan and Woodward (2010)
82.02 \pm 2.56	STM	Ryan and Woodward (2010)
87.47 \pm 2.36	NEATM	Masiero et al. (2011)
104.56 \pm 1.88	NEATM	Masiero et al. (2012)
87.34 \pm 9.06	NEATM	Pravec et al. (2012)
82.35 \pm 1.08	NEATM	Hasegawa et al. (2013)
88.00 \pm 9.00	NEATM	Ali-Lagoa et al. (2013)
84.79 \pm 1.56	NEATM	Masiero et al. (2014)
85.70 \pm 8.57	NEATM	Alí-Lagoa et al. (2016)
85.82 \pm 23.24	NEATM	Nugent et al. (2015)
71.59 \pm 18.01	NEATM	Nugent et al. (2016)
86.18 \pm 25.86	NEATM	Nugent et al. (2016)
75.77 \pm 15.15	NEATM	Alí-Lagoa et al. (2018)
87.25 \pm 17.45	NEATM	Alí-Lagoa et al. (2018)
95.95 \pm 9.59	NEATM	Alí-Lagoa et al. (2018)

authors acknowledge the use of the Virtual Observatory tools Miriade¹ (Berthier et al., 2008), TOPCAT², and STILTS³ (Taylor, 2005). This research used the SSOIS⁴ facility of the Canadian Astronomy Data Centre operated by the National Research Council of Canada with the support of the Canadian Space Agency (Gwyn et al., 2012).

References

- Alí-Lagoa, V., de León, J., Licandro, J., Delbó, M., Campins, H., Pinilla-Alonso, N., Kelley, M.S., 2013. Physical properties of B-type asteroids from WISE data. *A&A* 554, A71. doi:[10.1051/0004-6361/201220680](https://doi.org/10.1051/0004-6361/201220680), [arXiv:1303.5487](https://arxiv.org/abs/1303.5487).
- Alí-Lagoa, V., Licandro, J., Gil-Hutton, R., Cañada-Assandri, M., Delbo', M., de León, J., Campins, H., Pinilla-Alonso, N., Kelley, M.S.P., Hanuš, J., 2016. Differences between the Pallas collisional family and similarly sized B-type asteroids. *A&A* 591, A14. doi:[10.1051/0004-6361/201527660](https://doi.org/10.1051/0004-6361/201527660).
- Alí-Lagoa, V., Müller, T.G., Usui, F., Hasegawa, S., 2018. The AKARI IRC asteroid flux catalogue: updated diameters and albedos. *A&A* 612, A85. doi:[10.1051/0004-6361/201731806](https://doi.org/10.1051/0004-6361/201731806), [arXiv:1712.07496](https://arxiv.org/abs/1712.07496).
- Beauvalet, L., Marchis, F., 2014. Multiple asteroid systems (45) Eugenia and (87) Sylvia: Sensitivity to external and internal perturbations. *Icarus* 241, 13–25. doi:[10.1016/j.icarus.2014.06.004](https://doi.org/10.1016/j.icarus.2014.06.004).
- Berthier, J., Carry, B., Vachier, F., Eggl, S., Santerne, A., 2016. Prediction of transits of Solar system objects in Kepler/K2 images: an extension of the Virtual Observatory service SkyBoT. *MNRAS* 458, 3394–3398. doi:[10.1093/mnras/stw492](https://doi.org/10.1093/mnras/stw492).
- Berthier, J., Hestroffer, D., Carry, B., Durech, J., Tanga, P., Delbo, M., Vachier, F., 2008. A Service of Position and Physical Ephemerides Computation Dedicated to the Small Bodies of the Solar System. *LPI Contributions* 1405, 8374.

¹Miriade: <http://vo.imcce.fr/webservices/miriade/>

²TOPCAT: <http://www.star.bris.ac.uk/~mbt/topcat/>

³STILTS: <http://www.star.bris.ac.uk/~mbt/stilts/>

⁴SSOIS: <http://www.cadc-ccda.hia-iha.nrc-cnrc.gc.ca/en/ssois>

- 290 Berthier, J., Vachier, F., Marchis, F., Ďurech, J., Carry, B.,
 291 2014. Physical and dynamical properties of the main belt
 292 triple Asteroid (87) Sylvia. *Icarus* 239, 118–130. doi:[10.1016/j.icarus.2014.05.046](https://doi.org/10.1016/j.icarus.2014.05.046).
 293
- 294 Berthier, J., Vachier, F., Thuillot, W., Fernique, P., Ochsenbein,
 295 F., Genova, F., Lainey, V., Arlot, J.E., 2006. SkyBoT, a new
 296 VO service to identify Solar System objects, in: Gabriel, C.,
 297 Arviset, C., Ponz, D., Enrique, S. (Eds.), *Astronomical Data
 298 Analysis Software and Systems XV*, p. 367.
- 299 Bryson, J.F.J., Weiss, B.P., Getzin, B., Abrahams, J.N.H.,
 300 Nimmo, F., Scholl, A., 2019. Paleomagnetic Evidence for a
 301 Partially Differentiated Ordinary Chondrite Parent Asteroid.
 302 *Journal of Geophysical Research (Planets)* 124, 1880–1898.
 303 doi:[10.1029/2019JE005951](https://doi.org/10.1029/2019JE005951).
- 304 Carry, B., 2012. Density of asteroids. *Planet. Space Sci.* 73,
 305 98–118. doi:[10.1016/j.pss.2012.03.009](https://doi.org/10.1016/j.pss.2012.03.009).
- 306 Carry, B., Dumas, C., Fulchignoni, M., Merline, W.J., Berthier,
 307 J., Hestroffer, D., Fusco, T., Tamblyn, P., 2008. Near-Infrared
 308 Mapping and Physical Properties of the Dwarf-Planet Ceres.
 309 *A&A* 478, 235–244. doi:[10.1051/0004-6361:20078166](https://doi.org/10.1051/0004-6361:20078166).
- 310 Carry, B., Matter, A., Scheirich, P., Pravec, P., Molnar, L., Mot-
 311 tola, S., Carbognani, A., Jehin, E., Marciniak, A., Binzel,
 312 R.P., DeMeo, F., Birlan, M., Delbo, M., Barbotin, E.,
 313 Behrend, R., Bonnardel, M., Colas, F., Farissier, P., Fau-
 314 vaud, M., Fauvaud, S., Gillier, C., Gillon, M., Hellmich, S.,
 315 Hirsch, R., Leroy, A., Manfroid, J., Montier, J., Morelle, E.,
 316 Richard, F., Sobkowiak, K., Strajnic, J., Vachier, F., 2015.
 317 The small binary asteroid (939) Isberga. *Icarus* 248, 516–525.
 318 doi:[10.1016/j.icarus.2014.11.002](https://doi.org/10.1016/j.icarus.2014.11.002).
- 319 Carry, B., Vachier, F., Berthier, J., Marsset, M., Vernazza,
 320 P., Grice, J., Merline, W.J., Lagadec, E., Fienga, A., Con-
 321 rad, A., Podlewska-Gaca, E., Santana-Ros, T., Viikinkoski,
 322 M., Hanuš, J., Dumas, C., Drummond, J.D., Tamblyn, P.M.,
 323 Chapman, C.R., Behrend, R., Bernasconi, L., Bartczak, P.,
 324 Benkhaldoun, Z., Birlan, M., Castillo-Rogez, J., Cipriani,
 325 F., Colas, F., Drouard, A., Ďurech, J., Enke, B.L., Fau-
 326 vaud, S., Ferrais, M., Fetick, R., Fusco, T., Gillon, M., Jehin,
 327 E., Jorda, L., Kaasalainen, M., Keppler, M., Kryszczynska,
 328 A., Lamy, P., Marchis, F., Marciniak, A., Michalowski, T.,
 329 Michel, P., Pajuelo, M., Tanga, P., Vigan, A., Warner, B.,
 330 Witasse, O., Yang, B., Zurlo, A., 2019. Homogeneous internal
 331 structure of CM-like asteroid (41) Daphne. *A&A* 623, A132.
 332 doi:[10.1051/0004-6361/201833898](https://doi.org/10.1051/0004-6361/201833898), arXiv:1901.01890.
- 333 Carry, B., Vernazza, P., Vachier, F., Neveu, M., Berthier, J.,
 334 Hanuš, J., Ferrais, M., Jorda, L., Marsset, M., Viikinkoski,
 335 M., Bartczak, P., Behrend, R., Benkhaldoun, Z., Birlan, M.,
 336 Castillo-Rogez, J., Cipriani, F., Colas, F., Drouard, A., Dudz-
 337 iński, G.P., Desmars, J., Dumas, C., Ďurech, J., Fetick, R.,
 338 Fusco, T., Grice, J., Jehin, E., Kaasalainen, M., Kryszczynska,
 339 A., Lamy, P., Marchis, F., Marciniak, A., Michalowski,
 340 T., Michel, P., Pajuelo, M., Podlewska-Gaca, E., Rambaux,
 341 N., Santana-Ros, T., Storrs, A., Tanga, P., Vigan, A., Warner,
 342 B., Wieczorek, M., Witasse, O., Yang, B., 2021. Evidence for
 343 differentiation of the most primitive small bodies. *A&A* 650,
 344 A129. doi:[10.1051/0004-6361/202140342](https://doi.org/10.1051/0004-6361/202140342), arXiv:2103.06349.
- 345 Clement, M.S., Morbidelli, A., Raymond, S.N., Kaib, N.A., 2020.
 346 A record of the final phase of giant planet migration fossilized
 347 in the asteroid belt's orbital structure. *MNRAS* 492, L56–L60.
 348 doi:[10.1093/mnrasl/slz184](https://doi.org/10.1093/mnrasl/slz184), arXiv:1912.02833.
- 349 van Dam, M.A., Le Mignant, D., Macintosh, B., 2004. Perfor-
 350 mance of the Keck Observatory adaptive-optics system. *Ap-
 351 plied Optics* 43, 5458–5467.
- 352 DeMeo, F., Carry, B., Marchis, F., Birlan, M., Binzel, R.P., Bus,
 353 S.J., Descamps, P., Nedelcu, A., Busch, M., Bouy, H., 2011. A
 354 spectral comparison of (379) Huenna and its satellite. *Icarus*
 355 212, 677–681. doi:[10.1016/j.icarus.2011.02.002](https://doi.org/10.1016/j.icarus.2011.02.002).
- 356 DeMeo, F.E., Carry, B., 2014. Solar System evolution from com-
 357 positional mapping of the asteroid belt. *Nature* 505, 629–634.
- doi:[10.1038/nature12908](https://doi.org/10.1038/nature12908).
 358
- Drummond, J.D., Merline, W.J., Carry, B., Conrad, A., Tam-
 359 blyn, P., Enke, B., Christou, J., Dumas, C., Chapman, C.R.,
 360 Durda, D.D., Owen, W.M., Grundy, W.M., Reynolds, O.R.,
 361 Buckman, M.D., 2021. The orbit of asteroid (317) Roxane's
 362 satellite Olympias from Gemini, Keck, VLT and the SOR,
 363 and (22) Kalliope's Linus from the SOR. *Icarus* 358, 114275.
 364 doi:[10.1016/j.icarus.2020.114275](https://doi.org/10.1016/j.icarus.2020.114275).
 365
- Durda, D.D., Bottke, W.F., Enke, B.L., Merline, W.J., Asphaug,
 366 E., Richardson, D.C., Leinhardt, Z.M., 2004. The formation
 367 of asteroid satellites in large impacts: results from numeri-
 368 cal simulations. *Icarus* 170, 243–257. doi:[10.1016/j.icarus.2004.04.003](https://doi.org/10.1016/j.icarus.2004.04.003).
 369
- Elkins-Tanton, L.T., Weiss, B.P., Zuber, M.T., 2011. Chondrites
 370 as samples of differentiated planetesimals. *Earth and Plan-
 371 etary Science Letters* 305, 1–10. doi:[10.1016/j.epsl.2011.03.010](https://doi.org/10.1016/j.epsl.2011.03.010).
 372
- Emelyanov, N.V., Drozdov, A.E., 2020. Determination of the
 373 orbits of 62 moons of asteroids based on astrometric observa-
 374 tions. *MNRAS* 494, 2410–2416. doi:[10.1093/mnras/staa784](https://doi.org/10.1093/mnras/staa784).
 375
- Gwyn, S.D.J., Hill, N., Kavelaars, J.J., 2012. Ssos: A moving-
 376 object image search tool for asteroid precovery. *Publications
 377 of the Astronomical Society of the Pacific* 124, 579. doi:[10.1086/666462](https://doi.org/10.1086/666462).
 378
- Hasegawa, S., Müller, T.G., Kuroda, D., Takita, S., Usui,
 379 F., 2013. The Asteroid Catalog Using AKARI IRC Slow-
 380 Scan Observations. *PASJ* 65, 34. doi:[10.1093/pasj/65.2.34](https://doi.org/10.1093/pasj/65.2.34),
 381 arXiv:1210.7557. 382
- Herald, D., Gault, D., Anderson, R., Dunham, D., Frappa, E.,
 383 Hayamizu, T., Kerr, S., Miyashita, K., Moore, J., Pavlov, H.,
 384 Preston, S., Talbot, J., Timerson, B., 2020. Precise astrometry
 385 and diameters of asteroids from occultations - a data set of ob-
 386 servations and their interpretation. *MNRAS* 499, 4570–4590.
 387 doi:[10.1093/mnras/staa3077](https://doi.org/10.1093/mnras/staa3077), arXiv:2010.06086. 388
- Johnston, W., 2019. Binary Minor Planets Compilation V3.0.
 389 NASA Planetary Data System. doi:[10.26033/bb68-pw96](https://doi.org/10.26033/bb68-pw96). 390
- Lenzen, R., Hartung, M., Brandner, W., Finger, G., Hubin,
 391 N.N., Lacombe, F., Lagrange, A.M., Lehnert, M.D., Moor-
 392 wood, A.F.M., Mouillet, D., 2003. NAOS-CONICA first on
 393 sky results in a variety of observing modes. *SPIE* 4841, 944–
 394 952. 395
- Mainzer, A., Grav, T., Masiero, J., Bauer, J., Wright, E., Cutri,
 395 R.M., McMillan, R.S., Cohen, M., Ressler, M., Eisenhardt, P.,
 396 2011. Thermal Model Calibration for Minor Planets Observed
 397 with Wide-field Infrared Survey Explorer/NEOWISE. *ApJ*
 398 736, 100. doi:[10.1088/0004-637X/736/2/100](https://doi.org/10.1088/0004-637X/736/2/100). 399
- Marchis, F., Descamps, P., Berthier, J., Hestroffer, D., Vachier,
 400 F., Baek, M., Harris, A.W., Nesvorný, D., 2008. Main belt
 401 binary asteroidal systems with eccentric mutual orbits. *Icarus*
 402 195, 295–316. doi:[10.1016/j.icarus.2007.12.010](https://doi.org/10.1016/j.icarus.2007.12.010). 403
- Marchis, F., Vachier, F., Ďurech, J., Enriquez, J.E., Harris,
 404 A.W., Dalba, P.A., Berthier, J., Emery, J.P., Bouy, H., Mel-
 405 bourne, J., Stockton, A., Fassnacht, C.D., Dupuy, T.J., Stra-
 406 jnic, J., 2013. Characteristics and large bulk density of the
 407 C-type main-belt triple asteroid (93) Minerva. *Icarus* 224,
 408 178–191. doi:[10.1016/j.icarus.2013.02.018](https://doi.org/10.1016/j.icarus.2013.02.018). 409
- Margot, J.L., 2003. S/2003 (379) 1. *IAU Circ.* 8182, 1. 410
- Margot, J.L., Pravec, P., Taylor, P., Carry, B., Jacobson,
 411 S., 2015. Asteroid Systems: Binaries, Triples, and Pairs.
 412 Univ. Arizona Press. pp. 355–374. doi:[10.2458/azu_uapress_9780816532131-ch019](https://doi.org/10.2458/azu_uapress_9780816532131-ch019). 413
- Masiero, J.R., Grav, T., Mainzer, A.K., Nugent, C.R., Bauer,
 414 J.M., Stevenson, R., Sonnett, S., 2014. Main-belt Asteroids
 415 with WISE/NEOWISE: Near-infrared Albedos. *ApJ* 791, 121. 416
- Masiero, J.R., Mainzer, A.K., Grav, T., Bauer, J.M., Cutri,
 417 R.M., Dailey, J., Eisenhardt, P.R.M., McMillan, R.S., Spahr,
 418 T.B., Skrutskie, M.F., Tholen, D., Walker, R.G., Wright,
 419 420
- Masiero, J.R., Mainzer, A.K., Nugent, C.R., Bauer, J.M., Stevenson,
 421 R., Sonnett, S., 2014. Main-belt Asteroids with WISE/NEOWISE:
 422 Near-infrared Albedos. *ApJ* 791, 121. doi:[10.1088/0004-637X/791/2/121](https://doi.org/10.1088/0004-637X/791/2/121), arXiv:1406.6645. 423
- Masiero, J.R., Mainzer, A.K., Grav, T., Bauer, J.M., Cutri,
 424 R.M., Dailey, J., Eisenhardt, P.R.M., McMillan, R.S., Spahr,
 425 T.B., Skrutskie, M.F., Tholen, D., Walker, R.G., Wright,

- E.L., DeBaun, E., Elsbury, D., Gautier, IV, T., Gomillion, S., Wilkins, A., 2011. Main Belt Asteroids with WISE/NEOWISE. I. Preliminary Albedos and Diameters. *ApJ* 741, 68. doi:[10.1088/0004-637X/741/2/68](https://doi.org/10.1088/0004-637X/741/2/68).
- Masiero, J.R., Mainzer, A.K., Grav, T., Bauer, J.M., Cutri, R.M., Nugent, C., Cabrera, M.S., 2012. Preliminary Analysis of WISE/NEOWISE 3-Band Cryogenic and Post-cryogenic Observations of Main Belt Asteroids. *ApJ* 759, L8. doi:[10.1088/2041-8205/759/1/L8](https://doi.org/10.1088/2041-8205/759/1/L8), arXiv:1209.5794.
- McCord, T.B., Adams, J.B., Johnson, T.V., 1970. Asteroid vesta: Spectral reflectivity and compositional implications. *Science* 168, 1445–1447. doi:[10.1126/science.168.3938.1445](https://doi.org/10.1126/science.168.3938.1445).
- Morbidelli, A., Walsh, K.J., O'Brien, D.P., Minton, D.A., Bottke, W.F., 2015. The Dynamical Evolution of the Asteroid Belt. pp. 493–507. doi:[10.2458/azu_uapress_9780816532131-ch026](https://doi.org/10.2458/azu_uapress_9780816532131-ch026).
- Nugent, C.R., Mainzer, A., Bauer, J., Cutri, R.M., Kramer, E.A., Grav, T., Masiero, J., Sonnett, S., Wright, E.L., 2016. NEOWISE Reactivation Mission Year Two: Asteroid Diameters and Albedos. *AJ* 152, 63. doi:[10.3847/0004-6256/152/3/63](https://doi.org/10.3847/0004-6256/152/3/63), arXiv:1606.08923.
- Nugent, C.R., Mainzer, A., Bauer, J., Cutri, R.M., Grav, T., Kramer, E., Sonnett, S., Stevenson, R., Wright, E.L., 2015. NEOWISE Reactivation Mission Year One: Preliminary Asteroid Diameters and Albedos. *ApJ* 814, 117. doi:[10.1088/0004-637X/814/2/117](https://doi.org/10.1088/0004-637X/814/2/117), arXiv:1509.02522.
- Pajuelo, M., Carry, B., Vachier, F., Marsset, M., Berthier, J., Descamps, P., Merline, W.J., Tamblyn, P.M., Grice, J., Conrad, A., Storrs, A., Timerson, B., Dunham, D., Preston, S., Vigan, A., Yang, B., Vernazza, P., Fauvaud, S., Bernasconi, L., Romeuf, D., Behrend, R., Dumas, C., Drummond, J.D., Margot, J.L., Kervella, P., Marchis, F., Girard, J.H., 2018. Physical, spectral, and dynamical properties of asteroid (107) Camilla and its satellites. *Icarus* 309, 134–161. doi:[10.1016/j.icarus.2018.03.003](https://doi.org/10.1016/j.icarus.2018.03.003), arXiv:1803.02722.
- Pätzold, M., Andert, T.P., Asmar, S.W., Anderson, J.D., Barriot, J.P., Bird, M.K., Häusler, B., Hahn, M., Tellmann, S., Sierks, H., Lamy, P., Weiss, B.P., 2011. Asteroid 21 Lutetia: Low Mass, High Density. *Science* 334, 491. URL: <http://www.sciencemag.org/content/334/6055/491.abstract>, doi:[10.1126/science.1209389](https://doi.org/10.1126/science.1209389).
- Pravec, P., Harris, A.W., Kušnírák, P., Galád, A., Hornoch, K., 2012. Absolute magnitudes of asteroids and a revision of asteroid albedo estimates from WISE thermal observations. *Icarus* 221, 365–387. doi:[10.1016/j.icarus.2012.07.026](https://doi.org/10.1016/j.icarus.2012.07.026).
- Pravec, P., Scheirich, P., Kušnírák, P., Šarounová, L., Mottoola, S., Hahn, G., Brown, P.G., Esquerdo, G.A., Kaiser, N., Krzeminski, Z., Pray, D.P., Warner, B.D., Harris, A.W., Nolan, M.C., Howell, E.S., Benner, L.A.M., Margot, J.L., Galád, A., Holliday, W., Hicks, M.D., Krugly, Y.N., Tholen, D.J., Whiteley, R.J., Marchis, F., Degraff, D.R., Grauer, A., Larson, S., Velichko, F.P., Cooney, W.R., Stephens, R., Zhu, J., Kirsch, K., Dyvig, R., Snyder, L., Reddy, V., Moore, S., Gajdoš, Š., Világí, J., Masi, G., Higgins, D., Funkhouser, G., Knight, B., Slivan, S.M., Behrend, R., Grenon, M., Burki, G., Roy, R., Demeautis, C., Matter, D., Waelchli, N., Revaz, Y., Klotz, A., Rieugné, M., Thierry, P., Cotrez, V., Brunetto, L., Kober, G., 2006. Photometric survey of binary near-Earth asteroids. *Icarus* 181, 63–93. doi:[10.1016/j.icarus.2005.10.014](https://doi.org/10.1016/j.icarus.2005.10.014).
- Reddy, V., Dunn, T., Thomas, C.A., Moskovitz, N., Burbine, T., 2015. Mineralogy and Surface Composition of Asteroids. *Asteroids IV*, na.
- Rousset, G., Lacombe, F., Puget, P., Hubin, N.N., Gendron, E., Fusco, T., Arsenault, R., Charton, J., Feautrier, P., Gigan, P., Kern, P.Y., Lagrange, A.M., Madec, P.Y., Mouillet, D., Rabaud, D., Rabou, P., Stadler, E., Zins, G., 2003. NAOS, the first AO system of the VLT: on-sky performance. *SPIE* 4839, 140–149.
- Ryan, E.L., Woodward, C.E., 2010. Rectified Asteroid Albedos and Diameters from IRAS and MSX Photometry Catalogs. *AJ* 140, 933–943. doi:[10.1088/0004-6256/140/4/933](https://doi.org/10.1088/0004-6256/140/4/933).
- Scheeres, D.J., Britt, D., Carry, B., Holsapple, K.A., 2015. Asteroid Interiors and Morphology. Univ. Arizona Press. pp. 745–766. doi:[10.2458/azu_uapress_9780816532131-ch038](https://doi.org/10.2458/azu_uapress_9780816532131-ch038).
- Scheirich, P., Pravec, P., 2009. Modeling of lightcurves of binary asteroids. *Icarus* 200, 531–547. doi:[10.1016/j.icarus.2008.12.001](https://doi.org/10.1016/j.icarus.2008.12.001).
- Taylor, M.B., 2005. TOPCAT & STIL: Starlink Table/VOTable Processing Software, in: Shopbell, P., Britton, M., Ebert, R. (Eds.), *Astronomical Data Analysis Software and Systems XIV*, p. 29.
- Tedesco, E.F., Price, S.D., Egan, M.P., 2001. MIMPS, in: *AAS/Division for Planetary Sciences Meeting Abstracts #33*, p. 41.24.
- Usui, F., Hasegawa, S., Ishiguro, M., Müller, T.G., Ootsubo, T., 2014. A comparative study of infrared asteroid surveys: IRAS, AKARI, and WISE. *PASJ* 66, 56. doi:[10.1093/pasj/psu037](https://doi.org/10.1093/pasj/psu037), arXiv:1403.7854.
- Vachier, F., Berthier, J., Marchis, F., 2012. Determination of binary asteroid orbits with a genetic-based algorithm. *A&A* 543, A68. doi:[10.1051/0004-6361/201118408](https://doi.org/10.1051/0004-6361/201118408).
- Vernazza, P., Ferrais, M., Jorda, L., Hanuš, J., Carry, B., Marsset, M., Brož, M., Fetick, R., Viikinkoski, M., Marchis, F., Vachier, F., Drouard, A., Fusco, T., Birlan, M., Podlewska-Gaca, E., Rambaux, N., Neveu, M., Bartczak, P., Dudziński, G., Jehin, E., Beck, P., Berthier, J., Castillo-Rogez, J., Cipriani, F., Colas, F., Dumas, C., Ďurech, J., Grice, J., Kaasalainen, M., Kryszczynska, A., Lamy, P., Le Coroller, H., Marciniak, A., Michalowski, T., Michel, P., Santana-Ros, T., Tanga, P., Vigan, A., Witasse, O., Yang, B., Antonini, P., Audjean, M., Aurard, P., Behrend, R., Benkhaldoun, Z., Bosch, J.M., Chapman, A., Dalmon, L., Fauvaud, S., Hamanowa, H., Hamanowa, H., His, J., Jones, A., Kim, D.H., Kim, M.J., Krajewski, J., Labrevoir, O., Leroy, A., Livet, F., Molina, D., Montaigut, R., Oey, J., Payre, N., Reddy, V., Sabin, P., Sanchez, A.G., Socha, L., 2021. VLT/SPHERE imaging survey of the largest main-belt asteroids: Final results and synthesis. *A&A* 654, A56. doi:[10.1051/0004-6361/202141781](https://doi.org/10.1051/0004-6361/202141781).
- Weidenschilling, S.J., Paolicchi, P., Zappala, V., 1989. Do asteroids have satellites? *Asteroids II*, 643–658.
- Wizinowich, P.L., Acton, D.S., Lai, O., Gathright, J., Lupton, W., Stomski, Jr., P.J., 2000. Performance of the W.M. Keck Observatory Natural Guide Star Adaptive Optic Facility: the first year at the telescope, in: *SPIE*, pp. 2–13. doi:[10.1117/12.390368](https://doi.org/10.1117/12.390368).
- Yang, B., Hanuš, J., Carry, B., Vernazza, P., Brož, M., Vachier, F., Rambaux, N., Marsset, M., Chrenko, O., Ševeček, P., Viikinkoski, M., Jehin, E., Ferrais, M., Podlewska-Gaca, E., Drouard, A., Marchis, F., Birlan, M., Benkhaldoun, Z., Berthier, J., Bartczak, P., Dumas, C., Dudziński, G., Ďurech, J., Castillo-Rogez, J., Cipriani, F., Colas, F., Fetick, R., Fusco, T., Grice, J., Jorda, L., Kaasalainen, M., Kryszczynska, A., Lamy, P., Marciniak, A., Michalowski, T., Michel, P., Pajuelo, M., Santana-Ros, T., Tanga, P., Vigan, A., Witasse, O., 2020. Binary asteroid (31) Euphrosyne: ice-rich and nearly spherical. *A&A* 641, A80. doi:[10.1051/0004-6361/202038372](https://doi.org/10.1051/0004-6361/202038372), arXiv:2007.08059.
- Yang, B., Wahhaj, Z., Beauvalet, L., Marchis, F., Dumas, C., Marsset, M., Nielsen, E.L., Vachier, F., 2016. Extreme AO Observations of Two Triple Asteroid Systems with SPHERE. *ApJ* 820, L35. doi:[10.3847/2041-8205/820/2/L35](https://doi.org/10.3847/2041-8205/820/2/L35), arXiv:1603.04435.
- Zielenbach, W., 2011. Mass Determination Studies of 104 Large Asteroids. *AJ* 142, 120–128. doi:[10.1088/0004-6256/142/4/120](https://doi.org/10.1088/0004-6256/142/4/120).

Graphical Abstract

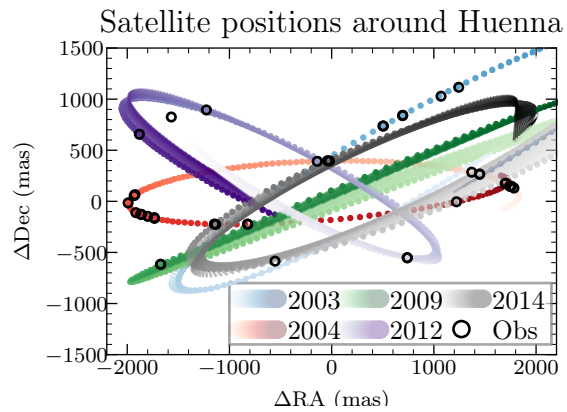
1

Dynamics of the binary asteroid (379) Huenna

2

Frédéric Vachier, Benoit Carry, Jérôme Berthier

3



4 Highlights

5 Dynamics of the binary asteroid (379) Huenna

6 Frédéric Vachier,Benoit Carry,Jérôme Berthier

- 7 • We gather 40 observations of Huenna and its satellite**
- 8 • We revise the published orbital elements of the satellite**
- 9 • The satellite is distant from Huenna, differing from other satellites of large asteroids**
- 10 • The density of Huenna is $1491 \pm 249 \text{ kg}\cdot\text{m}^{-3}$**